Optimal Energy Management and Control of an Industrial Microgrid with Plug-in Electric Vehicles

Marco Casini, Giovanni G. Zanvettor, Milica Kovjanic, Antonio Vicino *†

Abstract

An industrial microgrid (IMG) consists in a microgrid involving manufacturer plants which are usually equipped with distributed generation facilities, industrial electric vehicles, energy storage systems, etc. In this paper, the problem of IMG efficient operation in presence of plug-in electric vehicles is addressed. To this purpose, schedule of the different device operations of IMGs has to be optimally computed, minimizing the operation cost while guaranteeing electrical network stability and production constraints. Such a problem is formulated in a receding horizon framework involving dynamic optimal power flow equations. Uncertainty affecting plug-in electric vehicles is handled by means of a chance constraint approach. The obtained nonconvex problem is then approximately solved by exploiting suitable convex relaxation techniques. Numerical simulations have been performed showing computational feasibility and robustness of the proposed approach against increased penetration of electric vehicles.

keywords: Industrial microgrids, receding horizon control, dynamic optimal power flow, plug-in electric vehicles, chance constraints.

Nomenclature and abbreviations

Acronyms

CHP	Combined heat and power
CVaR	Conditional Value at Risk
DOPF	Dynamic optimal power flow
DG	Distributed generation
ESS	Energy storage system
FU	Factory unit
IMG	Industrial microgrid
PEV	Plug-in electric vehicle
PV	Photovoltaic

Mathematical notation

$\mathbb{R}^m$	Real space of dimension m
$\mathbb{S}^m$	Space of symmetric $(m \times m)$ matrices
v'	Transpose of vector v
$Tr(X)$	Trace of matrix X.
$[k, k+T]$	Time interval from step k to step $k+T$
$\underline{x}$ (underbar)	Lower bound of variable x
$\overline{x}$ (overbar)	Upper bound of variable x
x_i (subscript)	Value of variable x related to the bus i
$x(k)$ (time index)	Value of variable x at time k
$\mathcal{P}(e)$	Probability that event e occurs
$\mathbb{E}[x]$	Expected value of random variable x

*Dipartimento di Ingegneria dell'Informazione e Scienze Matematiche, Università di Siena, 53100 Siena, Italy.

†This work was supported by the Italian Ministero dell'Istruzione, dell'Università e della Ricerca (Grant No. PRIN 2017YKXYXJ).

Nomenclature

Δ	Sampling time
T	Horizon length
C_i^{CHP}	Cost of electricity production by the CHP system at bus i
C_i^B	Cost of heat production by the boiler at bus i
C^G	Cost of electricity from the main grid
$J_{[k,k+T]}$	Objective function to be minimized over the interval $[k, k+T]$
P_i^{CHP}	Active power generated by the CHP system at bus i
Q_i^{CHP}	Reactive power generated by the CHP system at bus i
η_i^{CHP}	Electric efficiency of the CHP system at bus i
c_i^{CHP}	Operation cost of the CHP system at bus i per unit of electrical power generated in a time slot
p^g	Gas price
P_i^B	Heat power produced by the boiler at bus i
η_i^B	Efficiency of the boiler at bus i
P_i^{PV}	Active power generated by the PV system at bus i
p^e	Electricity price
c_i^{PV}	Operation cost of the PV system at bus i per unit of electrical power generated in a time slot
P_i	Net active power injected at bus i
Q_i	Net reactive power injected at bus i
P_i^{S+}	ESS connected to bus i charge power
P_i^{S-}	ESS connected to bus i discharge power
P_i^F	Active power demand of the i-th factory unit
Q_i^F	Reactive power demand of the i-th factory unit
$P_{i,h}^{EV}$	Charge power of the h-th PEV connected to bus i
P_i^G	Active power generation at bus i
P_i^D	Active power demand at bus i
G_{ij}	Real part of the electrical admittance between bus i and bus j
B_{ij}	Imaginary part of the electrical admittance between bus i and bus j
V_i	Voltage magnitude at bus i
θ_{ij}	Voltage phase difference between bus i and bus j
α_i^{CHP}	Waste heat factor of the CHP system at bus i
R	Thermal power required by the IMG
E_i^S	Energy stored in the ESS connected to bus i
η_i^{S+}	Charging efficiency of ESS connected to bus i
η_i^{S-}	Discharging efficiency of ESS connected to bus i
$E_{i,h}^{EV}$	Energy stored in the battery of the h-th PEV connected to bus i
$\eta_{i,h}^{EV}$	Battery charging efficiency of the h-th PEV connected to bus i
$k_{i,h}^a$	Arrival time (starting charging time) of the h-th PEV connected to bus i
$k_{i,h}^d$	Departure time (stopping charging time) of the h-th PEV connected to bus i
K_i	Number of vehicles associated to bus i
$\mathcal{H}_{i,k}$	Set of indices of vehicles connected to bus i which are charging at time k
$\mathcal{H}_{i,[k,k+T]}$	Set of indices of vehicles connected to bus i whose minimum arrival time belongs to $[k, k+T]$
ϵ	Failure tolerance level
$\gamma_{i,h}(k)$	Binary random variable denoting if PEV h connected to bus i is charging at time k
$\Gamma_{i,h}$	Random vector containing $\gamma_{i,h}(k)$
$\Theta_{i,h}$	Support of random vector $\Gamma_{i,h}$
$\pi_{i,h}^{k^a}$	Vector of charging powers related to h-th PEV connected to bus i during $[\underline{k}_{i,h}^a, \overline{k}_{i,h}^a]$
$\Pi(k)$	Decision variable vector at time k
$\Pi^*(k)$	Optimal decision variable vector at time k
$\Pi_{[k,k+T]}$	Decision variable vector sequence in $[k, k+T]$
$\Pi_{[k,k+T]}^*$	Optimal decision variable vector sequence in $[k, k+T]$
k_{max}^d	Maximum departure time for all the vehicles belonging to $\mathcal{H}_{i,k} \cup \mathcal{H}_{i,[k,k+T]}$ for any i

1 Introduction

Due to the technological development of low carbon technologies such as renewable generation sources, local energy storage systems and electric vehicles, several issues came up to properly integrate these new features into existing power systems. In fact, the intermittent nature of the energy from renewables may affect negatively network stability and grid power quality. To this end, attention of the scientific community has focused on local communities, and in particular on microgrids [1–3]. In [4], a novel model of microgrid in the presence of renewables and electric vehicles has been presented, whereas in [5], a coordinated electric vehicle charging algorithm has been proposed to guarantee the power quality of the system. In this framework, secure grid operation under huge penetration of plug-in electric vehicles (PEVs) has been addressed [6, 7]. In [8], a battery swapping strategy to maximize the profit of a charging station has been developed, while in [9], a profit optimization procedure to manage an airport parking lot has been presented. Moreover, a peak-load reduction controller exploiting the coordinated response of photovoltaic (PV) systems, energy storage systems (ESSs) and PEVs has been developed in [10], whereas in [11] a smart charging control to minimize the operation cost under different user preferences is reported. Also, studies on sizing and siting of batteries, PV plants and electric vehicle charging stations have been carried out. In particular, optimal allocation of renewable sources and electric vehicles charging stations into a microgrid was addressed in [12]. In [13], an optimization method has been proposed for proper sizing and siting of DG units, energy storage systems and PEV charging stations, while an optimal storage sizing procedure to minimize the microgrid planning cost has been presented in [14].

Besides residential microgrids, recent years have witnessed a growing interest towards industrial microgrids (IMGs), i.e., microgrids involving manufacturing plants. In addition to the above mentioned features, this kind of microgrids has to take into account production loads, industrial electric vehicles, and possibly spatially distributed combined heat and electrical power generation sources [15]. In [16], an optimal microgrid planning for an industrial site in the presence of distributed generation (DG) plants has been proposed, while in [17] a multi-objective optimization of an industrial microgrid considering demand response, maximization of the total revenue, and total emission reduction, has been developed.

To guarantee a robust operation of microgrids, uncertainties affecting various aspects of the considered systems should be handled, as well. These uncertainties may affect directly the system behavior leading to possible violations of both technological and security constraints. In fact, since these constraints often depend on uncertain variables, a suitable modeling paradigm is needed to formulate them in probabilistic terms. A rigorous way to model this uncertainty is to make use of chance constraints [18, 19], which generally lead to complex formulations difficult to handle. In order to overcome this issue, several approximation techniques have been proposed, e.g., scenario-based [20] or distributionally chance constraint approaches [21]. For instance, a scenario-based approach has been introduced in [22] to guarantee network performance against uncertainties of power loads and electric vehicles arrivals, and in [23] to tackle uncertainty on renewable generation in a PEV parking lot.

In this paper, we consider an industrial microgrid involving a manufacturing plant composed of several spatially distributed buildings, hereafter referred to as *factory units* (FUs), connected to different buses. Such FUs perform different tasks of the production plan and some of them are assumed to be equipped with DG systems. In particular, PV systems coupled with electrical energy storage systems are considered. Further, we assume that FUs are provided with combined heat and power (CHP) systems able to produce electrical and heat power to be exchanged inside the IMG. In addition to CHP systems, heat power can also be generated through boilers. A fleet of plug-in electric vehicles is assumed to be assigned to each FU. Such vehicles can be of different types, ranging from picker to lift trucks, from bucket to delivery trucks [15]. The arrival (charging) time of each PEV is assumed to be uncertain, while the departure (plug-out) time is considered to be known in advance, since it is assumed to be scheduled in the FU production plan. In this setting, vehicle-to-grid power exchange will not be allowed. A sketch of the considered IMG is reported in Fig. 1.

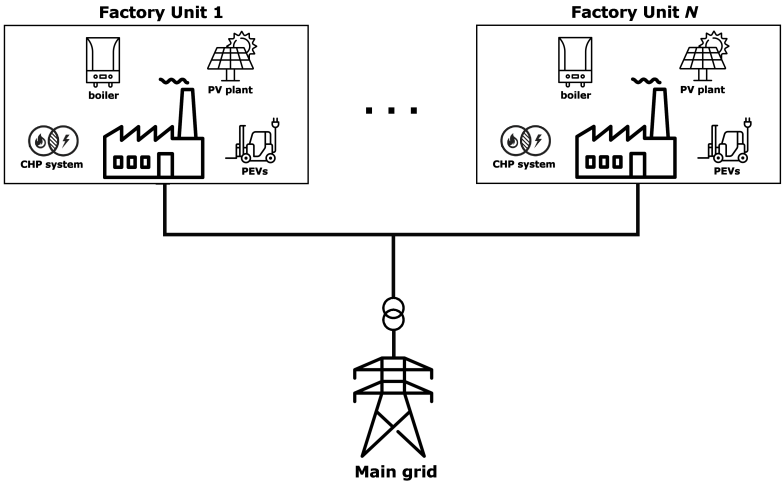

Figure 1: Sketch of an industrial microgrid.

The aim of the paper is to derive an optimal management and control policy for the IMG in order to minimize the energy bill, while satisfying electrical network stability constraints, heat and power exchange among FUs, and guaranteeing a suitable charge level to PEVs. Electricity and gas prices change over time and they are assumed to be known in advance. The optimization problem is formulated in a receding horizon framework [24,25], where at each time step a sequence of dynamic optimal power flow (DOPF) instances [26, 27] is solved. To tackle the uncertainty associated to each PEV, a chance constraint approach [18] is adopted. Due to power flow equations and chance constraints, the obtained optimization problem is nonconvex. Relaxations based on [28] and [21] make it possible to reformulate the nonconvex constraints as a set of linear matrix inequalities for power flow and chance constraints, respectively.

The novel contribution of this paper with respect to the existing literature can be summarized as follows:
i) the uncertainty related to PEVs is managed through a chance constraint approach. This solution allows one to consider also vehicles which are not in charge in the optimization problem;
ii) nonconvex constraints arisen by using chance constraints are relaxed by means of worst-case Conditional Value at Risk (CVaR) constraints [21], allowing for computationally feasible solution of the optimization problem.

Numerical simulations are performed to assess performance and computational feasibility of the proposed approach.

The paper is organized as follows. In Section 2, the problem of optimal control of an IMG is formulated, while in Section 3 the receding horizon approach is presented. A simulation case study is provided in Section 4. Conclusions and future developments are presented in Section 5.

2 Formulation of the Optimal Control of an IMG

In this paper, a discrete-time approach with sampling time Δ is considered. Let x be a generic variable, the notation $x(k)$ stands for the average value of x from time step k to $k+1$, i.e., from time $k\Delta$ to $(k+1)\Delta$. Let the number of buses involved in the IMG be denoted by N. By x_i we mean a generic variable x related to bus i.

The aim of this work is to minimize the overall cost of an IMG while respecting the physical and security constraints imposed by its components, i.e., power lines, DG facilities, ESSs, PEVs, etc. Moreover, operation constraints related to heat requirements and PEV charging set-points have to be respected, as well.

2.1 Objective Function

Let k denote the present time step and let T be the horizon length. The objective function to be minimized is defined as the sum of all the costs of the IMG over the time interval $[k\Delta,\, (k+T)\Delta]$. Electrical power can be generated by PV and CHP systems or it can be drawn from the main grid. Heat may be produced by boilers and CHP systems. Thus, for all the factory units, the cost of using CHP systems (C_i^{CHP}) and boilers (C_i^B) has to be taken into account in the objective function, as well as the cost of the electricity drawn from the main grid (C^G). Thus, the objective function to be minimized is:

$$J_{[k,k+T]} = \sum_{i=1}^{N} \sum_{t=k}^{k+T} C_i^{CHP}(t) + \sum_{i=1}^{N} \sum_{t=k}^{k+T} C_i^{B}(t) + \sum_{t=k}^{k+T} C^{G}(t) \ . \tag{1}$$

Let P_i^{CHP} be the electrical power produced by the i-th CHP system, and let η_i^{CHP} and p^g be the CHP efficiency and the gas price, respectively. Denoting by c_i^{CHP} the operation cost of the i-th CHP system per unit of electrical power generated in a time slot, the CHP cost can be expressed as:

$$C_i^{CHP}(k) = \frac{P_i^{CHP}(k)\Delta}{\eta_i^{CHP}}\, p^g(k) + P_i^{CHP}(k)\, c_i^{CHP} \ .$$

Let P_i^B be the heat power generated by the i-th boiler, then the corresponding cost is:

$$C_i^B(k) = \frac{P_i^B(k)\Delta}{\eta_i^B}\, p^g(k) \ ,$$

where η_i^B denotes the boiler efficiency.

Let us denote the net active and reactive power at bus i by P_i and Q_i, respectively. By convention, the slack bus is indexed by 1, so the net active and reactive powers drawn from the main grid correspond to P_1 and Q_1, respectively. Let $p^e(k)$ be the electricity price at time k, the overall electricity cost from the main grid can be written as:

$$C^G(k) = P_1(k)\Delta\, p^e(k) \ .$$

It is worthwhile to remark that $P_1(k)$ is the difference between the overall electric power needed by the IMG (for factory operation, power losses, PEV and ESS charging), and the electric power generated by CHP and PV systems.

In this work, to avoid arbitrage on electricity price, it is assumed that the IMG cannot inject electric power into the main grid, i.e., $P_1(k) \geq 0$ for all k.

2.2 Physical and Security Constraints

In this subsection, the physical and security constraints needed to ensure safe operation and physical stability of the IMG are defined.

First, the power balance equations are recalled. Let P_i^F be the active power demand of the factory unit connected to bus i and let the charge/discharge power of the i-th ESS be denoted by P_i^{S+} and P_i^{S-}, respectively. For a generic PEV h connected to bus i, $P_{i,h}^{EV}(k)$ represents the charge power at time k. Denoting by P_i^G and P_i^D the total generated and demanded active power at bus i, one has:

$$P_i^G(k) = P_i^{CHP}(k) + P_i^{PV}(k) + P_i^{S-}(k) \ ,$$

$$P_i^D(k) = P_i^F(k) + P_i^{S+}(k) + \sum_{h=1}^{K_i} P_{i,h}^{EV}(k) \ ,$$

where K_i is the set containing the indices of the vehicles connected to bus i.

The net active and reactive power at bus i can be written as [26, 27, 29]:

$$P_i(k) = V_i(k) \sum_{j=1}^{N} V_j(k) \big(G_{ij} \cos\theta_{ij}(k) - B_{ij} \sin\theta_{ij}(k) \big) \ ,$$

$$Q_i(k) = V_i(k) \sum_{j=1}^{N} V_j(k) \big(G_{ij} \sin\theta_{ij}(k) - B_{ij} \cos\theta_{ij}(k) \big) \ ,$$

where G_{ij} and B_{ij} are the real and imaginary part of the electrical admittance between bus i and j, V_i is the voltage magnitude at bus i, and θ_{ij} is the voltage phase angle difference between buses i and j. Thus, the active power balance equality constraint at bus i is:

$$P_i(k) - P_i^G(k) + P_i^D(k) = 0 \ .$$

The reactive powers of the PV systems and PEVs are neglected since these small generators are typically connected to the network through high quality grid-tie converters that feature a fixed power factor close to 1 [30]. The reactive power demand consists of the reactive power of the different FU loads. Denoting by Q_i^{CHP} and Q_i^F the reactive powers exchanged by the CHP system and the FU connected to bus i, the reactive power balance equation is:

$$Q_i(k) - Q_i^{CHP}(k) + Q_i^F(k) = 0 \ .$$

Let us now introduce the inequality constraints concerning network security, CHP and boiler systems, PV systems and PEVs. The network security constraints enforce limits on voltages at the different buses and capacities of the lines, the latter depending on physical properties of the lines [30]. No voltage limits are set on the slack bus since it is considered a fixed-voltage bus. As previously stated, we assume that the slack bus is labeled with $i = 1$. Let us denote by $P_{ij}(k)$ the power flowing from bus i to bus j in the k-th time slot. Network security constraints can be written as:

$$\underline{V}_i \leq V_i(k) \leq \overline{V}_i \ , \qquad i = 2, ..., N \ ,$$

and

$$|P_{ij}(k)| \leq \overline{P}_{ij} \ , \qquad i \neq j \ ,$$

while the slack bus constraints are:

$$0 \leq P_1(k) \leq \overline{P}_1 \ ,$$
$$\underline{Q}_1 \leq Q_1(k) \leq \overline{Q}_1 \ ,$$

where $\overline{P}_1$, $\underline{Q}_1$ and $\overline{Q}_1$ are given bounds.

Constraints on active and reactive power generation by the i-th CHP system are expressed as:

$$\underline{P}_i^{CHP} \leq P_i^{CHP}(k) \leq \overline{P}_i^{CHP} \ ,$$

$$\underline{Q}_i^{CHP} \leq Q_i^{CHP}(k) \leq \overline{Q}_i^{CHP} \ ,$$

while the heat power produced by a generic boiler i is constrained as:

$$0 \leq P_i^B(k) \leq \overline{P}_i^B \ .$$

Let E_i^S be the energy stored in the ESS connected to bus i, and let η_i^{S+} and η_i^{S-} be the corresponding charging/discharging efficiency, respectively. The constraints involving the ESS enforce limits on the charge/discharge power, the storage capacity and the energy balance. Thus:

$$0 \leq P_i^{S+}(k) \leq \overline{P}_i^{S+} \ ,$$

$$0 \leq P_i^{S-}(k) \leq \overline{P}_i^{S-} \ ,$$
$$\underline{E}_i^S \leq E_i^S(k) \leq \overline{E}_i^S \ ,$$
$$E_i^S(k) = E_i^S(k-1) + \eta_i^{S+} P_i^{S+}(k-1)\Delta - \frac{1}{\eta_i^{S-}} P_i^{S-}(k-1)\Delta.$$

Regarding PEVs, let us consider the generic vehicle h connected to bus i and denote by $E_{i,h}^{EV}$ the energy stored in its battery and by $\eta_{i,h}^{EV}$ the corresponding charging efficiency. The electrical vehicle charging process is represented by the following constraints:

$$E_{i,h}^{EV}(k) = E_{i,h}^{EV}(k-1) + \eta_{i,h}^{EV} P_{i,h}^{EV}(k-1)\Delta \ , \tag{2}$$

$$0 \leq P_{i,h}^{EV}(k) \leq \overline{P}_{i,h}^{EV} \ , \tag{3}$$

$$E_{i,h}^{EV}(k) \leq \overline{E}_{i,h}^{EV} \ . \tag{4}$$

2.3 Operational Constraints

Let $k_{i,h}^a$ and $k_{i,h}^d$ denote the time a generic PEV h connected to bus i starts and stops the charging process, respectively. We assume that the departure time $k_{i,h}^d$ is known, being it related to the factory production schedule, while the arrival time $k_{i,h}^a$ is uncertain. We also assume that the battery capacity at plug-in time is known. To assure that a vehicle is fully charged at the time it is plugged-out, the following constraint is introduced. It enforces the stored energy at departure time to be equal to the maximum battery capacity:

$$E_{i,h}^{EV}(k_{i,h}^d) = \overline{E}_{i,h}^{EV} \ . \tag{5}$$

In the considered setting, we assume that factory units can exchange heat among themselves, and that their CHP systems and boilers cooperate to satisfy the overall heat requirement. Denoting by α_i^{CHP} the waste factor that describes how much useful heat power is generated per electric power produced by the i-th CHP system, the constraint on the overall heat demand R of the IMG can be expressed as:

$$\sum_{i=1}^{N} \left(\alpha_i^{CHP} P_i^{CHP}(k) + P_i^B(k) \right) \geq R(k) \ .$$

3 Optimal Control Implementation

In this section, a receding horizon algorithm ensuring optimal operation of the IMG is derived. To this purpose, the objective function (1) has to be minimized in order to compute the optimal control sequence.

Let k denote the current time step. The arrival time of a vehicle is supposed to be uncertain, and therefore the constraint representing its charging process is meaningful only when that PEV is plugged into the network. For this reason, let us define $\mathcal{H}_{i,k} = \left\{ h : \ k_{i,h}^a \leq k \leq k_{i,h}^d \right\}$ as the set of indices identifying vehicles plugged into the i-th bus at time k. Since the cardinality of this set varies over time, the optimization procedure needs to be adapted at each time step. Therefore, an adaptive optimization problem need be formulated at each time step in order to find the best solution for the IMG operation.

Notice that $\mathcal{H}_{i,k}$ takes into account only the vehicles charging at time k, but it provides no information about the incoming ones. Ignoring such an aspect may lead to situations in which network safety constraints may be violated, e.g., due to voltage drops and/or power overloads caused by arrivals of vehicles in future steps. Thus, in order to prevent these events, a chance constrained approach is adopted to handle uncertainty affecting PEVs arrival times.

3.1 Uncertainty Modeling

The real arrival time of the h-th vehicle at bus i, $k^a_{i,h}$, is supposed to be a random variable with a bounded closed support $[\underline{k}^a_{i,h}, \overline{k}^a_{i,h}]$, and let us assume that the corresponding discrete distribution function is known.

To take into account the incoming vehicles, let us define the index set $\mathcal{H}_{i,[k,k+T]} = \left\{h : k < \underline{k}^a_{i,h} < k+T\right\}$ which contains the indices of the vehicles whose minimum arrival time falls into the prediction horizon. Notice that, by construction, sets $\mathcal{H}_{i,k}$ and $\mathcal{H}_{i,[k,k+T]}$ are disjoint, i.e., $\mathcal{H}_{i,k} \cap \mathcal{H}_{i,[k,k+T]} = \emptyset$, for all i and k.

Being the arrival time $k^a_{i,h}$ a random variable, also the evolution of the vehicle state of charge $E^{EV}_{i,h}$ becomes a random variable itself. So, to manage the charging process involving incoming vehicles, constraint (5) is replaced by the following chance constraint:

$$\mathcal{P}\Big(E^{EV}_{i,h}(k^d_{i,h}) \geq \overline{E}^{EV}_{i,h}\Big) \geq 1-\epsilon \ , \quad h \in \mathcal{H}_{i,[k,k+T]} \ , \tag{6}$$

where $0 < \epsilon < 1$ denotes a given failure tolerance level.

In order to model the uncertainty on the state of charge, let us define the binary random vector $\Gamma_{i,h}$ as

$$\Gamma_{i,h} = \Big[\gamma_{i,h}(\underline{k}^a_{i,h}), \ldots, \ \gamma_{i,h}(\overline{k}^a_{i,h})\Big]$$

where,

$$\gamma_{i,h}(k) = \begin{cases} 1 & \text{if} \quad k \geq k^a_{i,h} \\ 0 & \text{otherwise} \end{cases} \ , \ k = \underline{k}^a_{i,h}, \ldots, \overline{k}^a_{i,h}$$

describes if a vehicle is in charge at time k.

Combining (6) with $\Gamma_{i,h}$, the chance constraint can be rearranged as

$$\mathcal{P}\Bigg(\eta^{EV}_{i,h}\Delta\Big(\sum_{t=\underline{k}^a_{i,h}}^{\overline{k}^a_{i,h}} P^{EV}_{i,h}(t)\gamma_{i,h}(t) + \sum_{t=\overline{k}^a_{i,h}+1}^{k^d_{i,h}-1} P^{EV}_{i,h}(t)\Big) \geq \overline{E}^{EV}_{i,h} - E^{EV}_{i,h}(k^a_{i,h})\Bigg) \geq 1-\epsilon \ .$$

By using (2), the second sum can be rewritten as

$$\mathcal{P}\Bigg(\eta^{EV}_{i,h}\Delta \sum_{t=\underline{k}^a_{i,h}}^{\overline{k}^a_{i,h}} P^{EV}_{i,h}(t)\gamma_{i,h}(t) + E^{EV}_{i,h}(k^d_{i,h}) - E^{EV}_{i,h}(\overline{k}^a_{i,h}+1) \geq \overline{E}^{EV}_{i,h} - E^{EV}_{i,h}(k^a_{i,h})\Bigg) \geq 1-\epsilon \ ,$$

and finally

$$\mathcal{P}\left(\eta^{EV}_{i,h}\Delta\left(\pi^{t_a}_{i,h}\right)'\Gamma_{i,h} + \mathcal{E}^{EV}_{i,h} \geq 0\right) \geq 1-\epsilon, \tag{7}$$

where,

$$\pi^{k^a}_{i,h} = \Big[P^{EV}_{i,h}(\underline{k}^a_{i,h}), \ldots, \ P^{EV}_{i,h}(\overline{k}^a_{i,h})\Big]' ,$$

and

$$\mathcal{E}^{EV}_{i,h} = E^{EV}_{i,h}(k^d_{i,h}) - E^{EV}_{i,h}(\overline{k}^a_{i,h}+1) - \overline{E}^{EV}_{i,h} + E^{EV}_{i,h}(k^a_{i,h}).$$

Notice that, if the vehicle arrival time interval overlaps the current time, the arrival distribution $\Gamma_{i,h}$ can be replaced by the corresponding conditional distribution.

3.2 Optimization Problem Formulation

Let us define the command row vector $\Pi(k)$ as

$$\begin{aligned}\Pi(k) = \big[&P_{1,1}^{EV}(k), ..., P_{1,K_1}^{EV}(k), ..., P_{N,1}^{EV}(k), ..., P_{N,K_N}^{EV}(k),\\ &P_1^{S+}(k), ..., P_N^{S+}(k), P_1^{S-}(k), ..., P_N^{S-}(k),\\ &P_1^{CHP}(k), ..., P_N^{CHP}(k),\ Q_1^{CHP}(k), ..., Q_N^{CHP}(k),\\ &P_1^{B}(k), ..., P_N^{B}(k)\big]\ ,\end{aligned}$$

where K_i denotes the maximum number of vehicles related to bus i. Furthermore, let us introduce the vector $\Pi_{[k,k+T]}$ in order to collect the control sequence over the time interval $[k, k+T]$:

$$\Pi_{[k,k+T]} = [\Pi(k), \ldots,\ \Pi(k+T)]\,.$$

The DOPF problem can be formulated as reported in Problem 1.

Problem 1: Dynamic Optimal Power Flow over time horizon $[k, k+T]$.

$$\Pi^*_{[k,k+T]} = \underset{\Pi_{[k,k+T]}}{\operatorname{argmin}} \quad J_{[k,k+T]}$$

subject to:

$$\left.\begin{array}{ll}
P_i(t) = P_i^{CHP}(t) + P_i^{PV}(t) + P_i^{S-}(t) - P_i^{F}(t) - P_i^{S+}(t) - \sum_{h \in \mathcal{H}_{i,k} \cup \mathcal{H}_{i,[k,k+T]}} P_{i,h}^{EV}(t) & \\
Q_i(t) = Q_i^{CHP}(t) - Q_i^{F}(t) & \\
|P_{ij}(t)| \leq \overline{P}_{ij} \ , \quad j \neq i & \\
\underline{P}_i^{CHP} \leq P_i^{CHP}(t) \leq \overline{P}_i^{CHP} & \\
\underline{Q}_i^{CHP} \leq Q_i^{CHP}(t) \leq \overline{Q}_i^{CHP} & \\
0 \leq P_i^{B}(t) \leq \overline{P}_i^{B} & \\
0 \leq P_i^{S+}(t) \leq \overline{P}_i^{S+} & \\
0 \leq P_i^{S-}(t) \leq \overline{P}_i^{S-} & \\
\underline{E}_i^{S} \leq E_i^{S}(t) \leq \overline{E}_i^{S} &
\end{array}\right\} \begin{array}{l} t = k, \ldots, k+T, \\ i = 1, \ldots, N \end{array}$$

$$\left.\begin{array}{ll}
0 \leq P_1(t) \leq \overline{P}_1 & \\
\underline{Q}_1 \leq Q_1(t) \leq \overline{Q}_1 & \\
R(t) \leq \sum_{i=1}^{N} \left(\alpha_i^{CHP} P_i^{CHP}(t) + P_i^{B}(t) \right) &
\end{array}\right\} t = k, \ldots, k+T$$

$$\left.\begin{array}{ll}
\underline{V}_i \leq V_i(t) \leq \overline{V}_i &
\end{array}\right\} \begin{array}{l} t = k, ..., k+T, \\ i = 2, ..., N \end{array}$$

$$\left.\begin{array}{ll}
E_i^{S}(t) = E_i^{S}(t-1) + \eta_i^{S+} P_i^{S+}(t-1)\Delta - \frac{1}{\eta_i^{S-}} P_i^{S-}(t-1)\Delta &
\end{array}\right\} \begin{array}{l} t = k+1, ..., k+T, \\ i = 1, ..., N \end{array}$$

$$\left.\begin{array}{ll}
E_{i,h}^{EV}(t) = E_{i,h}^{EV}(t-1) + \eta_{i,h}^{EV} P_{i,h}^{EV}(t-1)\Delta & \\
0 \leq P_{i,h}^{EV}(t) \leq \overline{P}_{i,h}^{EV} & \\
E_h^{EV}(t) \leq \overline{E}_k^{EV} &
\end{array}\right\} \begin{array}{l} t = k_{i,h}^a + 1, ..., k_{i,h}^d, \\ i = 1, ..., N, \\ h \in \mathcal{H}_{i,k} \cup \mathcal{H}_{i,[k,k+T]} \end{array}$$

$$\left.\begin{array}{ll}
\mathcal{P}\left(\eta_{i,h}^{EV} \Delta \left(\pi_{i,h}^{y_a} \right)' \Gamma_{i,h} + \mathcal{E}_{i,h}^{EV} \geq 0 \right) \geq 1 - \epsilon &
\end{array}\right\} \begin{array}{l} i = 1, ..., N, \\ h \in \mathcal{H}_{i,[k,k+T]} \end{array}$$

$$\left.\begin{array}{ll}
E_{i,h}^{EV}(k_{i,h}^d) = \overline{E}_{i,h}^{EV} &
\end{array}\right\} \begin{array}{l} i = 1, ..., N, \\ h \in \mathcal{H}_{i,k} \ . \end{array}$$

Notice that, since $\mathcal{H}_{i,k} \cap \mathcal{H}_{i,[k,k+T]} = \emptyset, \ \forall i, \forall k$, the last two constraints of Problem 1 are mutually exclusive in the adaptive optimization procedure.

It is worthwhile to remark that this optimization problem is nonconvex. In fact, it involves power flow equations, which describe a highly nonlinear system, and chance constraints in which the feasible set is typically nonconvex.

From the optimal power flow perspective, the nonconvexity can be handled by using its dual formulation and by relaxing a rank constraint to obtain a convex problem. It has been proven that for radial networks like those considered in this paper, such a relaxation is exact, see [28] for details.

Regarding chance constrained optimization, in the next subsection a method to approximate such constraints is adopted.

3.3 Chance Constraint Approximation

In the literature, there exist mainly two approaches to approximate chance constraints. The first one regards scenario based methods, where a number of realizations of the random process is collected in order to approximate the original chance constraints [20, 31]. The drawback of this approach is that the number of samples needed increases considerably as the failure tolerance level decreases, leading to computationally demanding problems when satisfaction probability approaches 1. This feature may be dramatically amplified by the increasing number and dimension of the random vectors necessary to model uncertainty. In the considered setting, the number of PEVs employed into the IMG, and then the number of random vectors, amounts to tens or even hundreds, leading to computationally unfeasible problems.

The second approximation family involves robust optimization methods, where chance constraints are relaxed by exploiting stochastic properties of the uncertain variables involved. Hereafter, we refer to the technique proposed in [21], where the first and second order moments of the considered random variable are used to obtain a convex problem reformulation involving linear matrix inequalities. Then, such a problem can be efficiently solved by using standard optimization tools (e.g., [32–34]).

Thus, let us now focus on the random variable $\Gamma_{i,h}$, whose expected value is given by

$$\mathbb{E}[\Gamma_{i,h}] = \boldsymbol{\mu}_{i,h} = \left[\mu_{i,h}(\underline{k}^a_{i,h}), \ldots, \ \mu_{i,h}(\overline{k}^a_{i,h})\right]' ,$$

where

$$\mu_{i,h}(k) = \mathbb{E}[\gamma_{i,h}(k)] = P(\gamma_{i,h}(k) = 1) = P(k^a_{i,h} \leq k) \ .$$

Let $\Sigma_{i,h}$ denote the covariance matrix of $\Gamma_{i,h}$, one has:

$$\Sigma_{i,h} = \begin{bmatrix} \sigma_{i,h}(\underline{k}^a_{i,h}, \underline{k}^a_{i,h}) & \ldots & \sigma_{i,h}(\underline{k}^a_{i,h}, \overline{k}^a_{i,h}) \\ \vdots & \ddots & \vdots \\ \sigma_{i,h}(\overline{k}^a_{i,h}, \underline{k}^a_{i,h}) & \ldots & \sigma_{i,h}(\overline{k}^a_{i,h}, \overline{k}^a_{i,h}) \end{bmatrix} ,$$

where

$$\sigma_{i,h}(p,q) = \begin{cases} \mu_{i,h}(p)(1 - \mu_{i,h}(q)) & \text{if } p \leq q \\ \mu_{i,h}(q)(1 - \mu_{i,h}(p)) & \text{if } p > q. \end{cases}$$

The first and second order moments of $\Gamma_{i,h}$ can be combined as follows:

$$\Omega_{i,h} = \begin{bmatrix} \Sigma_{i,h} + \boldsymbol{\mu}_{i,h}\boldsymbol{\mu}'_{i,h} & \boldsymbol{\mu}_{i,h} \\ \boldsymbol{\mu}'_{i,h} & 1 \end{bmatrix} .$$

Let us refer to a generic h-th vehicle connected to bus i. In the following, for ease of notation, subscripts i and h are omitted. According to [21], chance constraint (7) can be approximated through CVaR and then replaced with the following set of convex constraints:

$$\begin{cases} \exists \beta \in \mathbb{R}, \ M \in \mathbb{S}^{(\overline{k}^a - \underline{k}^a + 2)}, \\ \exists \lambda \in \mathbb{R}^{(\overline{k}^a - \underline{k}^a + 1)}, \ \rho \in \mathbb{R}^{(\overline{k}^a - \underline{k}^a + 1)}, \\ \lambda \leq 0, \\ \rho \leq 0, \\ \beta + \frac{1}{\epsilon} Tr(M\Omega) \leq 0, \\ M + \sum\limits_{j=1}^{(\overline{k}^a - \underline{k}^a + 1)} W_j \lambda_j \succeq 0, \\ M + \sum\limits_{j=1}^{(\overline{k}^a - \underline{k}^a + 1)} W_j \rho_j - \\ \qquad \begin{bmatrix} 0 & -\frac{1}{2}\eta^{EV}\Delta\pi^{k^a} \\ -\frac{1}{2}\eta^{EV}\Delta\left(\pi^{k^a}\right)' & -\mathcal{E}^{EV} - \beta \end{bmatrix} \succeq 0 \ , \end{cases} \tag{8}$$

where $Tr(\cdot)$ is the trace operator and W_j are symmetric matrices of dimension $\overline{k}^a - \underline{k}^a + 1$. Such matrices are used to approximate the support Θ of Γ as:

$$\Theta \subseteq \Big\{ \Gamma \in \mathbb{R}^{(\overline{k}^a - \underline{k}^a + 1)} : \ [\Gamma',\ 1] W_j [\Gamma',\ 1]' \leq 0, \\ j = 1, \ldots, \overline{k}^a - \underline{k}^a + 1 \Big\} ,$$

where W_j are such that each entry of Γ must lie between 0 and 1.

3.4 Receding Horizon Implementation

Notice that the optimization Problem 1 does not take into account vehicles whose departure time falls outside the prediction horizon. To overcome this issue, a dynamic adaptation of the prediction horizon T is proposed as follows:

1. Let the nominal prediction horizon T be given.
2. At time k, let us check for each bus i if there is any PEV with index h such that $h \in \mathcal{H}_{i,k} \cup \mathcal{H}_{i,[k,k+T]}$:
   (a) if there is not any PEV belonging to $\mathcal{H}_{i,k} \cup \mathcal{H}_{i,[k,k+T]}$, then the prediction horizon remains unchanged;
   (b) if there are some vehicles belonging to $\mathcal{H}_{i,k} \cup \mathcal{H}_{i,[k,k+T]}$, the corresponding departure times $k^d_{i,h}$ have to be considered. Let us call k^d_{max} the maximum departure time for all the vehicles belonging to $\mathcal{H}_{i,k} \cup \mathcal{H}_{i,[k,k+T]}$. The prediction horizon has to be updated with the maximum value between k^d_{max} and T.

The overall receding horizon algorithm is reported in Algorithm 1.

Algorithm 1: Receding Horizon procedure

```
Let T_0 be the nominal prediction horizon;
Set k = 0;
Set T = T_0;
for i = 1 to N do
    for h ∈ H_{i,k} do
        Update the horizon as T = max{T, k^d_{i,h}};
        Add constraints (2)-(3)-(4)-(5) for vehicle h;
    end
    for h ∈ H_{i,[k,k+T_0]} do
        Update the horizon as T = max{T, k^d_{i,h}};
        Add constraints (2)-(3)-(4)-(8) for vehicle h;
    end
end
Solve Problem 1 to obtain Π*_{[k,k+T]};
Apply command Π*(k);
k = k + 1;
Repeat from step 3
```

4 Numerical simulations

In this section, an IMG is simulated in order to test the effectiveness and the computational feasibility of the proposed approach.

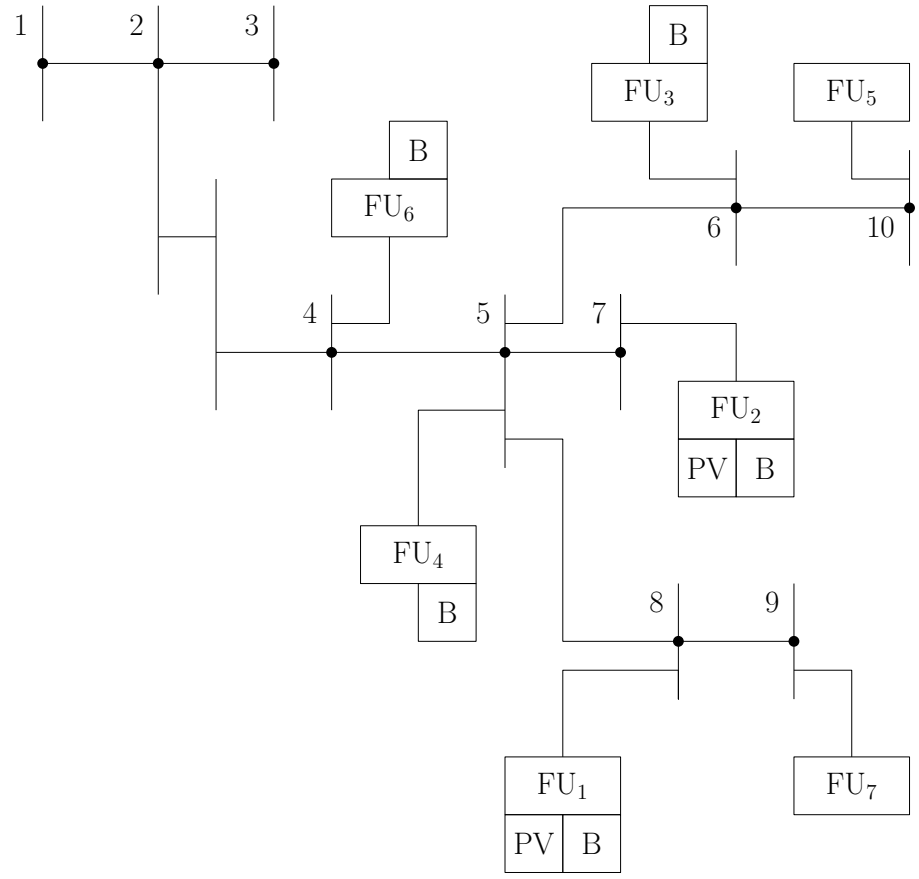

Figure 2: Structure of the considered 10-bus industrial microgrid. "B" denotes boilers while "PV" photovoltaic plants.

4.1 Simulation setup

Simulations have been performed over three days with a sampling time $\Delta = 1$ hour, a standard prediction horizon $T_0 = 4$ hours and a chance constraint failure tolerance level $\epsilon = 0.1$.

An IMG composed of 10 buses and 7 FUs is considered, see Fig. 2. Factory units are referred to as FU_1 , ..., FU_7 and they may be equipped with CHP systems, boilers, PV plants and PEVs. DG facilities installed in each FU are summarized in Table 1.

Technical data regarding DG systems and PEVs are taken from [15]. Data of CHP systems, that is, maximum and minimum active power generation, electric efficiency, waste heat factor and operational cost are reported in Table 2, while technical data regarding boilers are given in Table 3.

Each PV plant is assumed to be coupled with an ESS able to store the power in excess into batteries. Technical specifications about storage systems are reported in Table 4.

Forecasts of factory load patterns, PV generation and heat requirements are assumed to be

Table 1: Distributed generation facilities assigned to each factory unit.

	$\mathbf{FU}_1$	$\mathbf{FU}_2$	$\mathbf{FU}_3$	$\mathbf{FU}_4$	$\mathbf{FU}_5$	$\mathbf{FU}_6$	$\mathbf{FU}_7$
CHP system	X	X	X	X	X	X	X
Boiler	X	X	X	X		X	
PV plant	X	X					

Table 2: CHP systems technical data.

	$\mathbf{FU}_1$	$\mathbf{FU}_2$	$\mathbf{FU}_3$	$\mathbf{FU}_4$	$\mathbf{FU}_5$	$\mathbf{FU}_6$	$\mathbf{FU}_7$
$\underline{P}^{CHP}[kW]$	150	90	9	9	3	3	3
$\overline{P}^{CHP}[kW]$	1500	900	90	90	30	30	30
η^{CHP}	0.27	0.34	0.31	0.31	0.30	0.30	0.26
α^{CHP}	1.84	1.20	1.85	1.85	2.05	2.05	1.71
$c^{CHP}[\frac{€}{kW}]$	0.006	0.009	0.013	0.013	0.018	0.018	0.015

Table 3: Boilers technical data.

	$\mathbf{FU}_1$	$\mathbf{FU}_2$	$\mathbf{FU}_3$	$\mathbf{FU}_4$	$\mathbf{FU}_6$
$\overline{P}^{B}\ [kW]$	800	400	80	80	80
η^{B}	0.8	0.85	0.85	0.85	0.83

Table 4: ESS technical data.

	$\mathbf{FU}_1$	$\mathbf{FU}_2$
$\underline{E}^{S}\ [kWh]$	0	0
$\overline{E}^{S}\ [kWh]$	1000	250
$\overline{P}^{S+}\ [kW]$	350	100
$\overline{P}^{S-}\ [kW]$	350	100
$\underline{\eta}^{S+}$	0.92	0.9
$\underline{\eta}^{S-}$	0.92	0.9

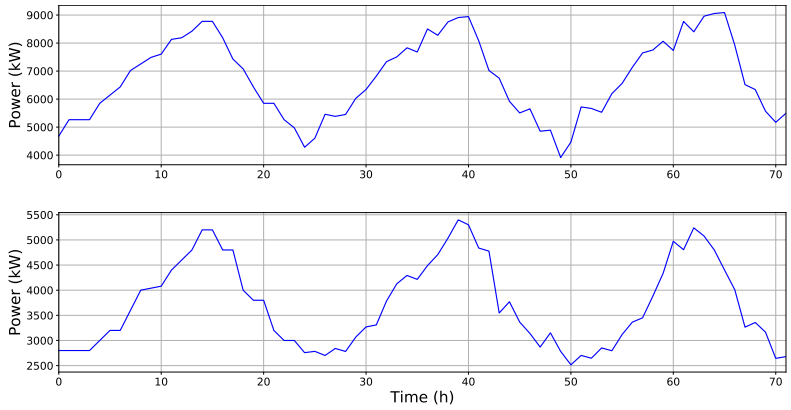

Figure 3: Top: overall FU electrical load. Bottom: overall heat requirement.

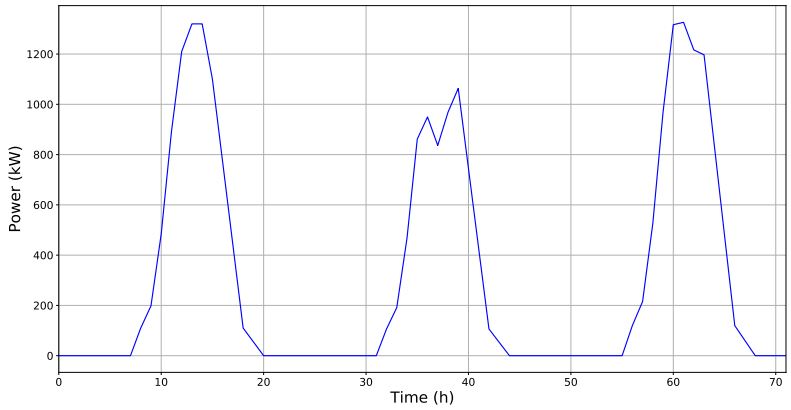

Figure 4: Overall photovoltaic generation.

known enough time in advance. The overall factory electrical load and heat requirement are depicted in Fig. 3, whereas the overall PV generation is reported in Fig. 4. The IMG is supposed to be equipped with three types of PEVs (light service vehicles, heavy service vehicles and large industrial vehicles) each one divided in two subclasses. Technical data on PEV charging systems are reported in Table 5, while in Table 6, the number of vehicles assigned to each FU is reported.

Daily arrival and departure schedules of PEVs are reported in Table 7. The actual arrival times of vehicles are taken from a symmetric triangular distribution with a support of 4 hours.

For all buses, the nominal voltage magnitude is set to $230\,V$, and the safety limits are given by $\pm 10\%$ of the nominal value. The slack bus is constrained to draw at most 6500 kW of active power from the grid and the constraints on the reactive power are set to $\overline{Q_i} = -\underline{Q_i} = 3150\ kVAR$. All the other buses of the network are treated as load buses.

Electricity and gas prices have been taken from the Italian electricity market [35] and they are depicted in Fig. 5. Notice that, electricity price changes every hour while gas price is updated once a day.

4.2 Simulation Results

The results obtained by simulating the considered IMG show that the proposed control strategy is able to efficiently manage all the grid components.

From the electrical point of view, in Fig. 6 (top), one may observe the relationship among CHP production, PV generation and main grid power consumption. As expected, when the electricity price is low, the IMG power is mostly drawn from the main grid. In Fig. 6 (bottom), the total

Table 5: PEVs technical data.

Vehicle Type	η^{PEV}	$\overline{E}^{PEV}$	$\overline{P}^{PEV}$
Light Service 1	0.88	16	23
Light Service 2	0.88	24	4
Heavy Service 1	0.9	170	24
Heavy Service 2	0.92	85	14
Large Industrial 1	0.95	100	100
Large Industrial 2	0.95	200	200

Table 6: Number of vehicles for each FU.

	$\mathbf{FU}_1$	$\mathbf{FU}_2$	$\mathbf{FU}_3$	$\mathbf{FU}_4$	$\mathbf{FU}_5$	$\mathbf{FU}_6$	$\mathbf{FU}_7$
Light Service 1	5	4	3	3	3	3	3
Light Service 2	10	4	4	4	4	4	4
Heavy Service 1	5	1	0	0	0	0	0
Heavy Service 2	8	4	0	0	0	0	0
Large Industrial 1	5	3	3	0	0	0	0
Large Industrial 2	5	2	0	0	0	0	0

Table 7: Arrival and departure time of vehicles.

Vehicle Type	Charging cycles					
	1			2		
	$\underline{t_a}$	$\overline{t_a}$	t_d	$\underline{t_a}$	$\overline{t_a}$	t_d
Light Service 1	16:00	20:00	6:00	-	-	-
Light Service 2	16:00	20:00	6:00	-	-	-
Heavy Service 1	17:00	21:00	5:00	-	-	-
Heavy Service 2	16:00	20:00	6:00	-	-	-
Large Industrial 1	9:00	13:00	15:00	18:00	22:00	6:00
Large Industrial 2	10:00	14:00	16:00	20:00	0:00	5:00

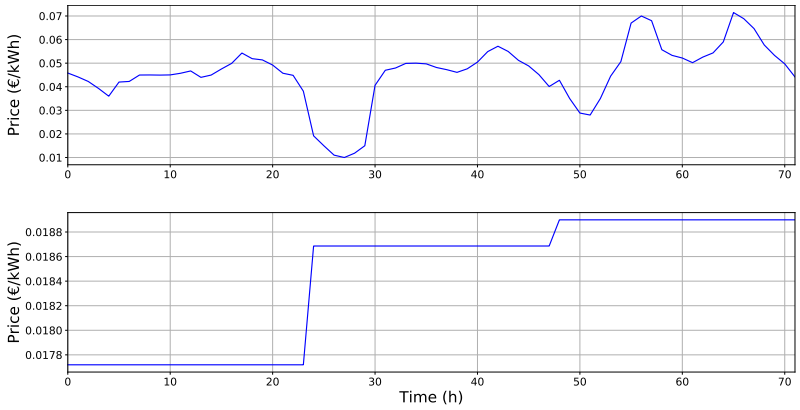

Figure 5: Top: electricity price. Bottom: gas price.

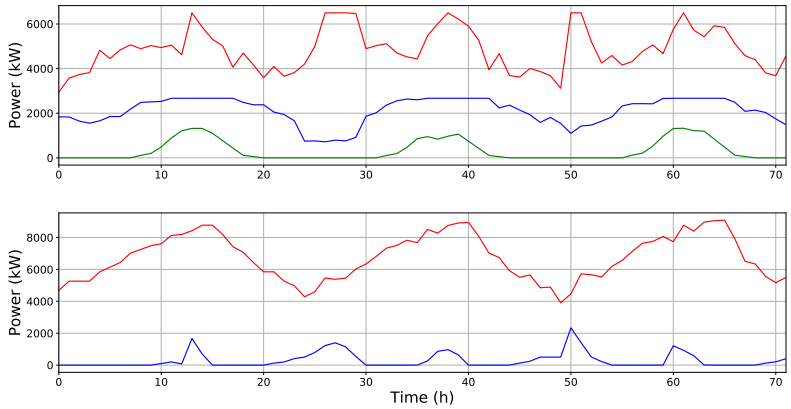

Figure 6: Electrical power side of the grid. Top: overall electrical power supply. Overall CHP generation (blue), PV production (green), main grid power consumption (red). Bottom: overall electrical power demand. Overall FU load (red) and PEV demand (blue).

FU electrical demand is reported, as well as the overall PEV charging profile, while in Fig. 7, the state of charge of the storages related to FU_1 and FU_2 is depicted.

Moving the attention on the heat demand reported in Fig. 8, CHP systems and boilers are employed to satisfy such constraint. In particular, boilers are mainly used both when CHP systems saturate and when producing electrical power through them is not convenient, e.g., around time 25. Concerning the overall heat generation, it can be noticed that the total produced heat always coincides with the requirement except around time 57, when the heat produced by CHP systems exceeds the overall requirement.

In Fig. 9, voltage magnitudes of buses 4, 6 and 8 are depicted. It can be observed that voltage magnitudes remain in the working range at all times. The largest fluctuations can be observed at bus 8 (red), which is connected to the most demanding FU, i.e. FU_1.

In order to evaluate the performance of the proposed approach, a benchmark consisting in Algorithm 1 without chance constraints (i.e., without lines 9-12) is considered. The two algorithms have been compared over a three-day simulation, showing similar overall costs, as reported in Table 8. On the other hand, to assess the robustness of the two procedures, an increased PEV penetration has been considered. Under this new setting, the benchmark is no more capable to satisfy grid constraints when the number of vehicles increases of about 30%, while the proposed chance constraint approach is able to guarantee an optimal grid operation even for a number of vehicles more than doubled. Hence, thanks to the adopted chance constraint control strategy, the optimization procedure can suitably manage the incoming vehicles with a consequent improvement

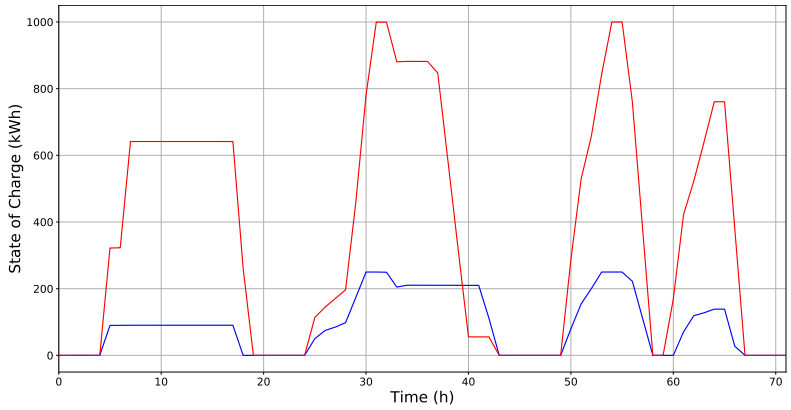

Figure 7: State of charge of ESS at FU_1 (red) and FU_2 (blue).

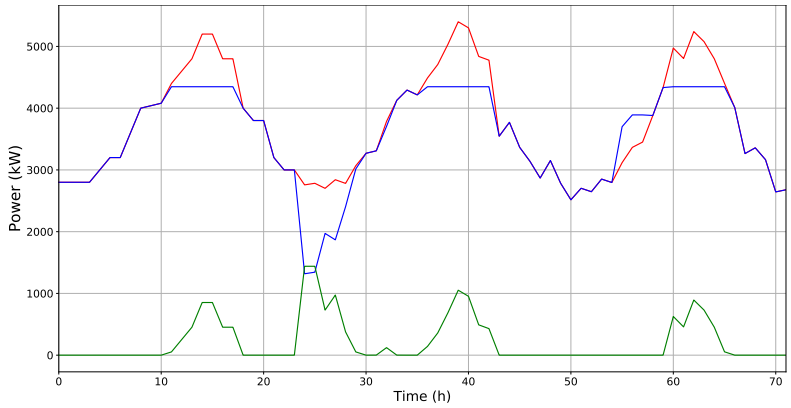

Figure 8: IMG heat requirement (red), overall CHP thermal generation (blue) and boiler heat production (green).

of the grid security.

In Fig. 10, the electrical power side of the IMG under double penetration of vehicles is depicted. In this setup, the grid is highly stressed. Indeed, the slack bus and the CHP systems reach often their saturation limits due to the heavy demand of PEVs. However, the proposed algorithm enforces the feasibility of the IMG network by spreading the PEV charging process over the whole plug-in time.

Regarding computational aspects, the proposed algorithm results to be largely tractable. In fact, the time needed by an iteration amounts to about 7 seconds.[1]

5 Conclusions

A receding horizon approach to the optimal control of an IMG in presence of PEVs has been presented. To deal with the uncertainty affecting the arrival times of PEVs, a chance constraint approach has been devised and a suitable relaxation technique has been adopted. Simulations involving a 10-bus industrial microgrid have been performed. The proposed approach has been compared with a deterministic method which does not employ chance constraints. Results show that the overall energy bill is similar for both approaches. However, the proposed method outperforms the benchmark when looking at robustness regarding PEV penetration. In fact, the

[1]Simulations have been carried out using CVXPY [36] to model the problem and MOSEK [32] to solve it on a Intel(R) Core(TM) i7-7700 CPU @3.60 GHz with 32 GB of RAM.

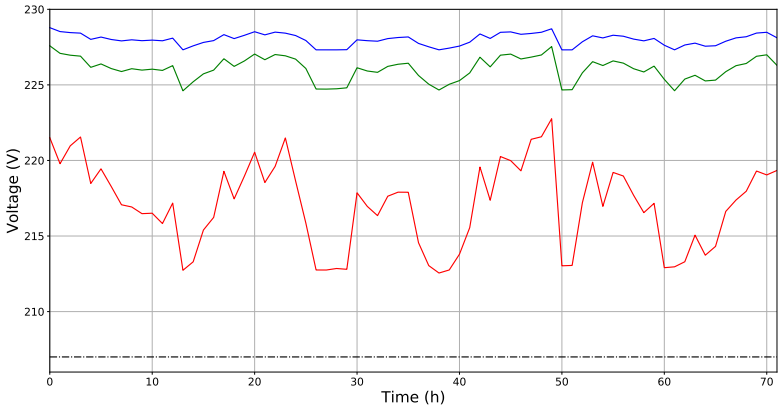

Figure 9: Voltages at buses 4 (blue), 6 (green) and 8 (red).

Table 8: Grid operation costs [€] over three days.

	Day 1	Day 2	Day 3	Total
Proposed procedure	8643.56	8457.12	9953.39	27054.07
Benchmark	8644.99	8461.27	9956.88	27063.13

benchmark is able to handle PEV increase of about 30%, after that network stability is no more guaranteed, while the algorithm based on chance constraint can manage PEV growth of more than 100%, showing better robustness capabilities.

Future developments may involve the use of different kind of techniques for dealing with uncertainty, like for instance, scenario-based approaches. Moreover, uncertainties on vehicle departure times and on other aspects of the IMG (e.g., uncertain FU load profile and uncertain PV generation forecasts) can be considered as well.

References

[1] A. Hirsch, Y. Parag, and J. Guerrero, "Microgrids: A review of technologies, key drivers, and outstanding issues," *Renewable and Sustainable Energy Reviews*, vol. 90, pp. 402 – 411, 2018.

[2] Z. Shuai, Y. Sun, Z. J. Shen, W. Tian, C. Tu, Y. Li, and X. Yin, "Microgrid stability: Classification and a review," *Renewable and Sustainable Energy Reviews*, vol. 58, pp. 167–179, 2016.

[3] S. Parhizi, H. Lotfi, A. Khodaei, and S. Bahramirad, "State of the art in research on microgrids: A review," *IEEE Access*, vol. 3, pp. 890–925, 2015.

[4] M. Zhang and J. Chen, "The energy management and optimized operation of electric vehicles based on microgrid," *IEEE Transactions on Power Delivery*, vol. 29, pp. 1427–1435, June 2014.

[5] S. Deilami, "Online coordination of plug-in electric vehicles considering grid congestion and smart grid power quality," *Energies*, vol. 11, no. 9, 2018.

[6] R. C. Green, L. Wang, and M. Alam, "The impact of plug-in hybrid electric vehicles on distribution networks: a review and outlook," in *IEEE PES General Meeting*, pp. 1–8, July 2010.

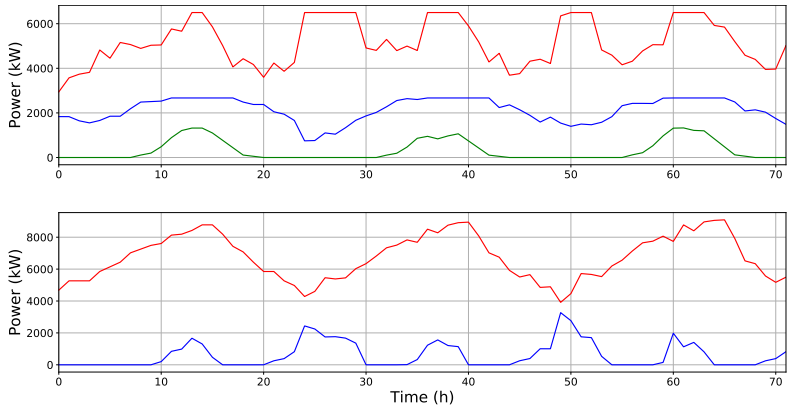

Figure 10: Electrical power side of the grid with double penetration of vehicles. Top: overall electrical power supply. Overall CHP generation (blue), PV production (green), main grid power consumption (red). Bottom: overall electrical power demand. Overall FU load (red) and PEV demand (blue).

[7] M. A. López, S. Martín, J. A. Aguado, and S. de la Torre, "V2G strategies for congestion management in microgrids with high penetration of electric vehicles," *Electric Power Systems Research*, vol. 104, pp. 28–34, 2013.

[8] M. R. Sarker, H. Pandžić, and M. A. Ortega-Vazquez, "Optimal operation and services scheduling for an electric vehicle battery swapping station," *IEEE Transactions on Power Systems*, vol. 30, pp. 901–910, March 2015.

[9] M. Maigha and M. L. Crow, "A transactive operating model for smart airport parking lots," *IEEE Power and Energy Technology Systems Journal*, vol. 5, pp. 157–166, Dec 2018.

[10] K. Mahmud, M. J. Hossain, and G. E. Town, "Peak-load reduction by coordinated response of photovoltaics, battery storage, and electric vehicles," *IEEE Access*, vol. 6, pp. 29353–29365, 2018.

[11] J. Clairand, J. Rodrìguez-Garcìa, and C. Àlvarez-Bel, "Smart charging for electric vehicle aggregators considering users' preferences," *IEEE Access*, vol. 6, pp. 54624–54635, 2018.

[12] M. R. Mozafar, M. H. Moradi, and M. H. Amini, "A simultaneous approach for optimal allocation of renewable energy sources and electric vehicle charging stations in smart grids based on improved GA-PSO algorithm," *Sustainable Cities and Society*, vol. 32, pp. 627–637, 2017.

[13] O. Erdinç, A. Taşcıkaraoğlu, N. G. Paterakis, İ. Dursun, M. C. Sinim, and J. P. S. Catalão, "Comprehensive optimization model for sizing and siting of dg units, ev charging stations, and energy storage systems," *IEEE Transactions on Smart Grid*, vol. 9, pp. 3871–3882, July 2018.

[14] I. Alsaidan, A. Khodaei, and Wenzhong Gao, "Distributed energy storage sizing for microgrid applications," in *2016 IEEE/PES Transmission and Distribution Conference and Exposition (T D)*, pp. 1–5, May 2016.

[15] S. Y. Derakhshandeh, A. S. Masoum, S. Deilami, M. A. S. Masoum, and M. E. Hamedani Golshan, "Coordination of generation scheduling with pevs charging in industrial microgrids," *IEEE Transactions on Power Systems*, vol. 28, pp. 3451–3461, Aug 2013.

[16] M. Naderi, S. Bahramara, Y. Khayat, and H. Bevrani, "Optimal planning in a developing industrial microgrid with sensitive loads," *Energy Reports*, vol. 3, pp. 124 – 134, 2017.

[17] M. Choobineh and S. Mohagheghi, "A multi-objective optimization framework for energy and asset management in an industrial microgrid," *Journal of Cleaner Production*, vol. 139, pp. 1326 – 1338, 2016.

[18] A. Ben-Tal, L. El Ghaoui, and A. Nemirovski, *Robust optimization*, vol. 28. Princeton University Press, 2009.

[19] J. R. Birge and F. Louveaux, *Introduction to stochastic programming*. Springer Science & Business Media, 2011.

[20] G. C. Calafiore and M. C. Campi, "The scenario approach to robust control design," *IEEE Transactions on Automatic Control*, vol. 51, pp. 742–753, May 2006.

[21] S. Zymler, D. Kuhn, and B. Rustem, "Distributionally robust joint chance constraints with second-order moment information," *Mathematical Programming*, vol. 137, pp. 167–198, Feb 2013.

[22] R. Leou, C. Su, and C. Lu, "Stochastic analyses of electric vehicle charging impacts on distribution network," *IEEE Transactions on Power Systems*, vol. 29, pp. 1055–1063, May 2014.

[23] M. Honarmand, A. Zakariazadeh, and S. Jadid, "Self-scheduling of electric vehicles in an intelligent parking lot using stochastic optimization," *Journal of the Franklin Institute*, vol. 352, no. 2, pp. 449 – 467, 2015. Special Issue on Control and Estimation of Electrified vehicles.

[24] W. H. Kwon and S. H. Han, *Receding horizon control: model predictive control for state models*. Springer Science & Business Media, 2006.

[25] J. H. Lee, "Model predictive control: Review of the three decades of development," *International Journal of Control, Automation and Systems*, vol. 9, no. 3, p. 415, 2011.

[26] D. Kothari and I. Nagrath, *Modern Power System Analysis*. Tata McGraw-Hill Publishing Company, 2003.

[27] A. Wood, B. Wollenberg, and G. Sheblé, *Power Generation, Operation, and Control*. Wiley, 2013.

[28] S. H. Low, "Convex relaxation of optimal power flow-part i: Formulations and equivalence," *IEEE Transactions on Control of Network Systems*, vol. 1, pp. 15–27, March 2014.

[29] J. Grainger and W. Stevenson, *Power system analysis*. McGraw-Hill series in electrical and computer engineering: Power and energy, McGraw-Hill, 1994.

[30] A. Giannitrapani, S. Paoletti, A. Vicino, and D. Zarrilli, "Optimal allocation of energy storage systems for voltage control in LV distribution networks," *IEEE Transactions on Smart Grid*, vol. 8, pp. 2859–2870, Nov 2017.

[31] J. Luedtke and S. Ahmed, "A sample approximation approach for optimization with probabilistic constraints," *SIAM Journal on Optimization*, vol. 19, no. 2, pp. 674–699, 2008.

[32] MOSEK ApS, *The MOSEK optimization toolbox for MATLAB manual. Version 8.1.*, 2017.

[33] J. Sturm, "Using SeDuMi 1.02, a Matlab toolbox for optimization over symmetric cones," *Optimization Methods and Software*, vol. 11–12, pp. 625–653, 1999.

[34] K. C. Toh, M. J. Todd, and R. H. Tütüncü, "SDPT3 - a Matlab software package for semidefinite programming, version 1.3," *Optimization Methods and Software*, vol. 11, no. 1-4, pp. 545–581, 1999.

[35] Gestore Mercati Energetici, "Andamento dei prezzi e dei volumi," 2018. Online: http://www.mercatoelettrico.org.

[36] S. Diamond and S. Boyd, "CVXPY: A Python-embedded modeling language for convex optimization," *Journal of Machine Learning Research*, vol. 17, no. 83, pp. 1–5, 2016.